

Investigations of supersonic vortex cores above and behind of a wing

A. M. Kharitonov*, A. E. Lutsky**, A. M. Shevchenko*

**Khristianovich Institute of Theoretical and Applied Mechanics
Institutskaya 4/1, 630090 Novosibirsk, Russia*

***Keldysh Institute of Applied Mathematics RAS
Miusskaya sq. 4, 125047 Moscow, Russia*

Abstract

A review of a comprehensive experimental study of supersonic longitudinal vortices is presented. A flow-field over the lee-side of a high sweep delta wing were examined at Mach number range from 2 to 4, and angles of attack up to 22 deg. Vortex wakes behind of a rectangular wing was studied at Mach numbers of 3 and 4, and angles of attack up to 20 deg. Two sets of computations using three-dimensional compressible Euler and Navier-Stokes equations were created. In Euler computations a "jet-like" vortex was obtained, as against a "wake-like" type which was observed in the Navier-Stokes solutions and the experiments.

1. Introduction

The renewed interest in the high-speed transport program has created a need for information on wing-tip vortices, their characteristics, and subsequent propagation into the downstream wake. Changes in the Mach number and angles of attack can induce global reconstruction of flowfield, which differ in the number, size, and positions of streamwise vortices and internal shock waves. Advanced manoeuvrable flying vehicles are equipped by lifting surfaces, a low-aspect-ratio delta wing being one element of these surfaces. Therefore, a detailed study of the structure of a supersonic flow around a delta wing ensures better understanding of typical features of the flow around real aerodynamic configurations. A large variety of flow regimes¹⁻⁵ and a comparatively simple geometry offer a possibility of using the delta wing as a test case for numerical methods developed for computing complicated spatial flows.

On the other hand, propagation of the vortex sheet in a cocurrent flow is also very important. Thus, vortices generated by lifting surfaces of a flying vehicle can produce an adverse effect on the flow around another vehicle in the wake of the first one.

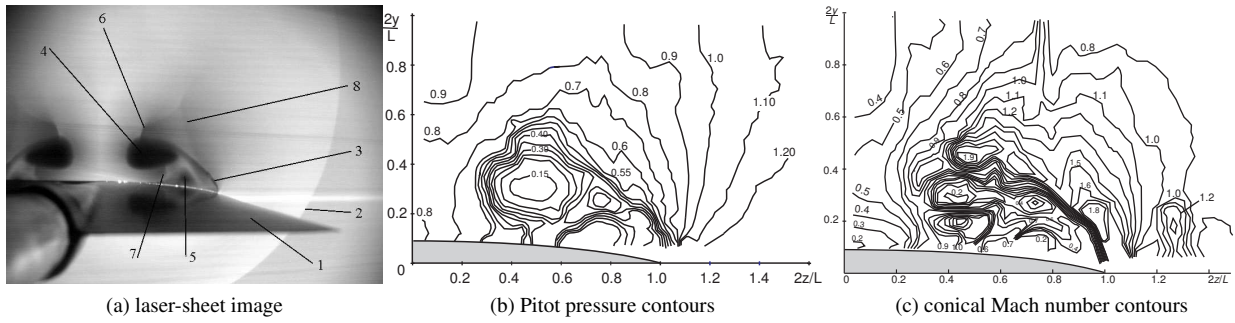
To date, wake-vortex systems were subjects for many studies in Europe and USA. European projects on trailing vortices like EUROWAKE, CWAKE, AWIATOR, FARWAKE have been supported in this conjuncture. Nevertheless, from the fundamental point of view, all the work in this field dealt with low Mach number flows. However, trailing vortices are compressible even for transonic commercial airplanes. A few studies were implemented to obtain the flow characteristics in the core of the streamwise vortex and its propagation and dissipation at supersonic speeds.⁶

In view of this, the Institute of Theoretical and Applied Mechanics (ITAM) and the Keldysh Institute of Applied Mathematics (KIAM) performed a comprehensive study of flow regimes around the delta wing^{4,5,7} and possibilities of their numerical simulation.⁸ Recently^{9,10} an experimental and numerical study of the flowfield in supersonic vortex wake behind of rectangular wing was performed in ITAM and KIAM.

A brief review of these results is presented in the paper.

2. Lee-side flow above of a delta wing

The experiments were performed with two delta wings with sharp leading and trailing edges. The wings had leading edge sweep angles of 73 and 78 deg with 3 percent symmetric parabolic profiles. Experiments were conducted in the supersonic blow-down wind tunnel T-313 of the Institute of Theoretical and Applied Mechanics of the Russian Academy of Sciences with the test section dimensions of $0.6 \times 0.6 \times 2$ m. The test conditions were varied in a range of Mach numbers $M = 2 - 4$, corresponding unit Reynolds numbers $Re_1 = (26 - 56) \cdot 10^6 \text{ m}^{-1}$, and angles of attack up to 22 deg. The method of soot-oil coating was used to visualize the limiting streamlines on the model surface.


 Figure 1: Experimental flowfield at $M = 3$, $\alpha = 14$ deg

Visualization of the spatial flow pattern was conducted with the laser light sheet imaging technique. Five-hole pressure probe technique was used to measure Pitot pressure, local Mach number, flow angularities over the lee-side of a delta wing.

It should be noted that the flow in the vicinity of the wing, strictly speaking, is not conical. All available experimental data,^{1-5,7} however, testify that the flow is close to conical. This means that the characteristic lines of convergence and divergence on the wing surface are close to straight lines. The distributions of flow parameters over the relative coordinates are usually within the measurement error. The positions of the internal shock waves, vortices, and other flow features in different cross sections of the wing, which are determined in normalized coordinates, are in good agreement. For this reason, the axial Mach number M_ξ and the conical Mach number M_C defined as

$$M_\xi = \frac{xM_x + yM_y + zM_z}{\sqrt{x^2 + y^2 + z^2}}; \quad M_C = \sqrt{M^2 - M_\xi^2} = \sqrt{\frac{(yM_z - zM_y)^2 + (zM_x - xM_z)^2 + (xM_y - yM_x)^2}{x^2 + y^2 + z^2}}$$

were chosen to analyze the flow under study. Here M_x, M_y, M_z are the Mach numbers based on the corresponding projections of the vector of local flow velocity onto the coordinate axes x, y , and z . The use of the conical Mach number is preferable to the use of the crossflow Mach number $(M_y^2 + M_z^2)^{1/2}$. For instance, we have $M_C = 0$ on the conical vortex centerline, whereas $(M_y^2 + M_z^2)^{1/2} \neq 0$.

The results obtained allowed one to significantly expand the knowledge of the specific features of the flow around a delta wing, to find new flow regimes on the leeward side of the wing, to locate the boundaries of these flow regimes. Fig. 1 shows typical experimental results for the case $M = 3$, $\alpha = 14$ deg. On the laser sheet image the model 1 and the bow shock wave 2 are clearly visible. The vortex sheet 3 separates from the leading edge and roll-up of the primary vortex 4. The primary vortex generates local minimum in leeside pressure distribution. The slight increase in pressure between its minimum and the leading edge can be large enough to force the cross-flow boundary layer to separate and form a secondary vortex 5. At sufficiently high angles of attack crossflow shock waves above the primary vortex 6 and under one 7 could be observed. The shock wave under the primary vortex is apparently caused by the fact that supersonic cross-flow under the primary vortex is decelerated toward the secondary separation and becomes subsonic flow through passing a locally normal shock. The necessity of turning two supersonic crossflows, which are directed from the leading edge of the wing to the plane of central symmetry toward each other, in the axial direction, causes the onset of crossflow shocks above the pair of the primary vortices. Fig. 1a also shows the formation of the λ -shock 8 above the vortex sheet and the primary vortex. The core of the primary vortex is the region with low values of density, total pressure, and conical Mach number. Correspondingly, the contours of Pitot pressure and conical Mach number have a closed form in this region. The maximum gradients of conical Mach number are observed at the vortex core boundaries.

Figure 2 shows Pitot pressure and Mach number distributions across the core of the primary vortex. The values M_{zc} and M_{yc} can be interpreted as radial and circumferential components of the local total Mach number. It is seen that not only Pitot pressure and conical Mach number decrease in the center of the vortex core, but also the axial Mach number is does. As a consequence, a minimum of the total Mach number is observed. Thus, a "wake-like" vortex is revealed. The boundary of the vortex core can be defined on maxima in conical Mach number.

The analysis of the results allows detecting the influence of the angle of attack, of the sweep angle, and of the free-stream Mach number on the topology of the cross-flow (Fig. 3). With increasing angle of attack, the vortex core increases in size and moves farther from the model surface. The distance between the cores decreases. The vortex sheet and the core of primary vortex occupy a greater area above the lee side of the wing. The same evolution of the

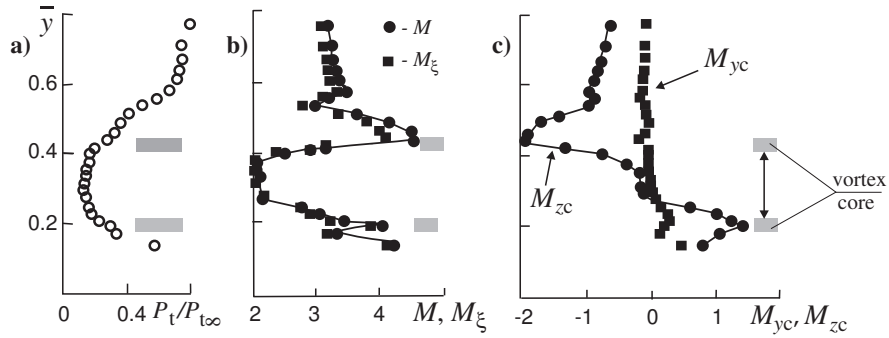


Figure 2: Pitot pressure and Mach numbers distributions across the vortex core ($M = 3$, $\alpha = 14$ deg, $2z/L = 0.45$)

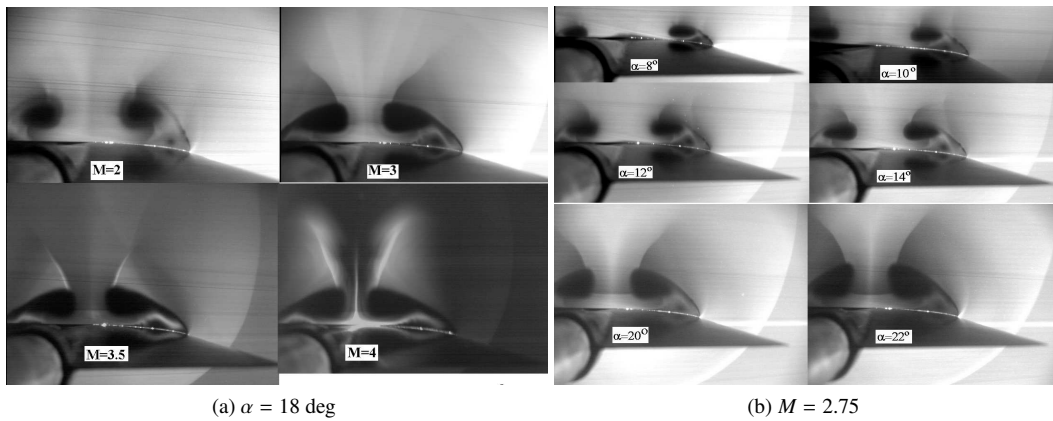


Figure 3: Influence of Mach number and angle of attack on the lee-side flow

vortex cores was observed within the entire examined range of Mach numbers. With increasing Mach number for a fixed value of angle of attack, the primary vortex core becomes flatter, it approaches the wing and occupies a large area above its surface. The distance between the vortex core decreases with increasing Mach number.

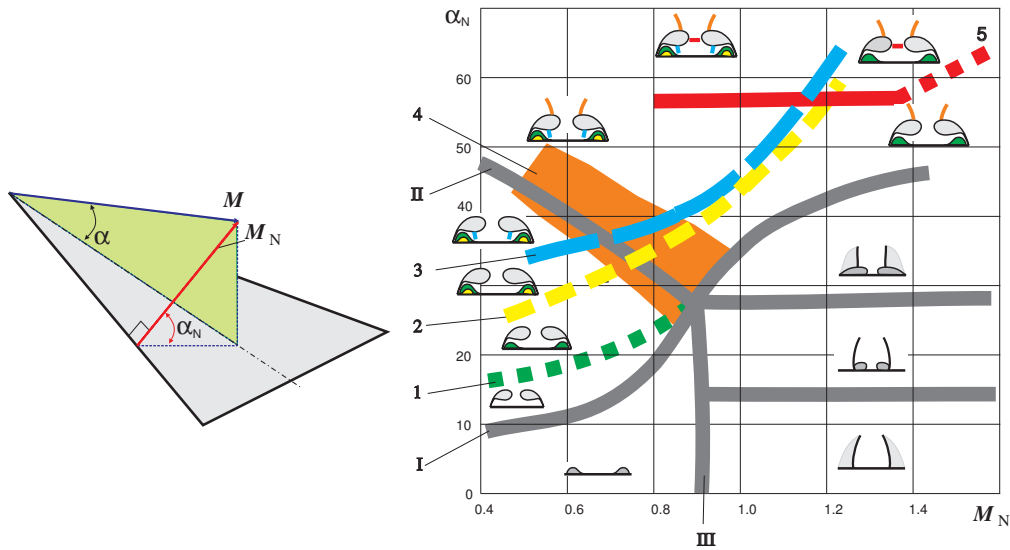


Figure 4: Delta wing flow regimes chart

The flow regimes chart is shown in Fig. 4 with the normal Mach number M_N and the normal angle of attack α_N as the coordinates. The gray shaded curves marked by the Roman numerals represent the boundaries of various flow

regimes defined by Wood and Miller.² The Arabic numerals mark the boundaries obtained through the analysis of flow visualization results presented here. In Fig. 4, the green boundary 1 divides the flow regimes with secondary separation and without it. The yellow line 2 is the boundary of flow regimes with tertiary separation. The region above the blue boundary line 3 corresponds to the flow regimes in which a shock wave appears under the primary vortex. The region below one conformed to shock-free flows. It is seen in Fig. 4 that the boundary 3 is close to the boundary line 2 for the onset of tertiary separation. The brown region 4 of flow regimes corresponds to the transition from the flow regime without the shock wave above of the primary vortex to the regimes with this shock wave. It was obtained that the shock wave between of the primary vortices disappears for free-stream Mach numbers $M > 3.5$. This transition is indicated by the red boundary line 5, which divides flow regimes with formation of this shock wave and without one.

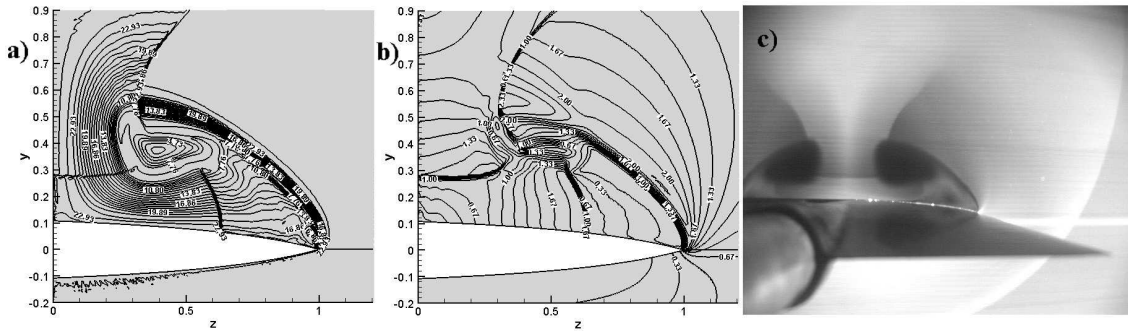


Figure 5: Cross-flow at $M = 2.75$, $\alpha = 20$ deg: (a) total pressure contours; (b) conical Mach number contours; (c) laser light-sheet image

As an example, Fig. 5 shows a comparison of numerical and experimental results obtained for the 78 deg sweep wing at $M = 2.75$ and $\alpha = 20$ deg. Numerical modeling was conducted in the KIAM. 3D steady Euler equations were solved using the space-marching method. Numerical simulations involved solving a system of three-dimensional steady Euler equations of a hyperbolic type. The technique considered was implemented within the framework of the zonal (multidomain) approach.¹¹

It is seen that computations fairly accurately predict the main inviscid features of the lee-side flow over the wing. The core of the primary vortex is the region with low values of total pressure and conical Mach number. The maximum gradients of conical Mach number are observed at the vortex-core boundaries. The positions of internal shock waves are determined from a typical inflection and closeness of isolines. As is seen from Fig. 5, the computations contain shock waves under, above, and between the pair of primary vortices. On each shock wave, the conically supersonic flow becomes conically subsonic.

Thus, the comparison shows that the inviscid approximation offers an adequate prediction of the positions of the vortex sheet, primary vortex, and internal shock waves above and under the primary vortex, and also incipience of a shock wave between the pair of primary vortices. Secondary and tertiary separations cannot be modeled by the Euler equations. A comparison of the results of the present study and the data¹²⁻¹⁶ shows that simulation of the flow by the Euler equations allows one to predict the "lower" boundary of flow regimes with emergence of internal shock waves, i.e., if the internal shock wave is not observed in Euler computations, it is ("most probably") absent in the real flow.

3. Vortex wake behind of a rectangular wing

3.1 Research techniques

The experiments were conducted in the supersonic wind tunnel T-313 of ITAM SB RAS. A wing-tip vortex is generated by a rectangular half-wing with a span of 300 mm. A hexahedral airfoil has a chord length of 80 mm, a half-angle of 8 deg. The wing was mounted on the test section floor at the tunnel centerline. The vortex generator could be set at different angles of attack in the range from -30 to 30 deg. A wing-tip vortex is generated by an unswept semispan slender wing with a span of 300 mm (Fig. 6). A hexahedral airfoil has a chord length of 80 mm, a half-angle of 8 deg. The wing was mounted on the test section floor at the tunnel centerline. The vortex generator could be set at different angles of attack in the range from -30 to 30 deg.

Flow visualization techniques included a multiple spark shadow photograph of 1–5 microsecond spark duration and a laser light sheet imaging technique. Three 5-hole conical pressure probes were used to measure local Mach number, Pitot pressure and flow angularity in the core of the wing-tip vortex and its vicinity. Quantitative flowfield

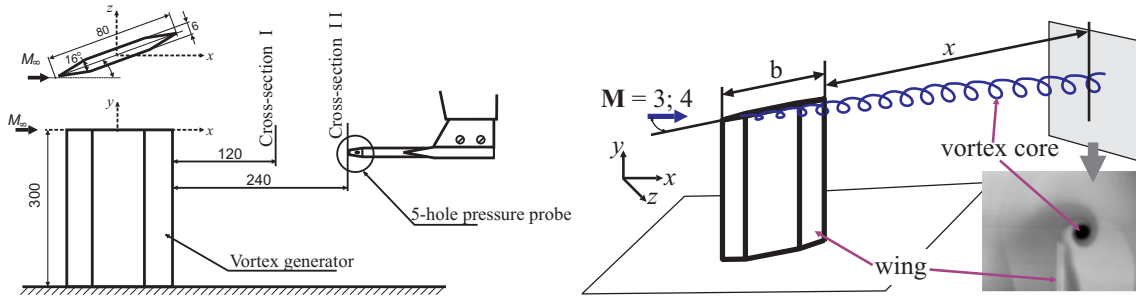


Figure 6: Sketch of experiment.

measurements and laser sheet visualization were performed at two cross-sections at the distance of 120 mm and 240 mm downstream from the wing trailing edge. The present experiments were performed at Mach numbers of 3 and 4. Vortex generator was mounted at angles of attack $\alpha = 5, 10, 15$ and 20 deg.

The numerical studies included solving three-dimensional steady Euler equations and unsteady laminar Navier-Stokes equations. A zonal approach was used.¹¹ A 16-block grid with 9336600 cells and improved geometric properties was used at presented study. The computations were performed with the use of advanced parallelization algorithms on a multiprocessor system RSC-4 in KIAM.

3.2 Results and discussion

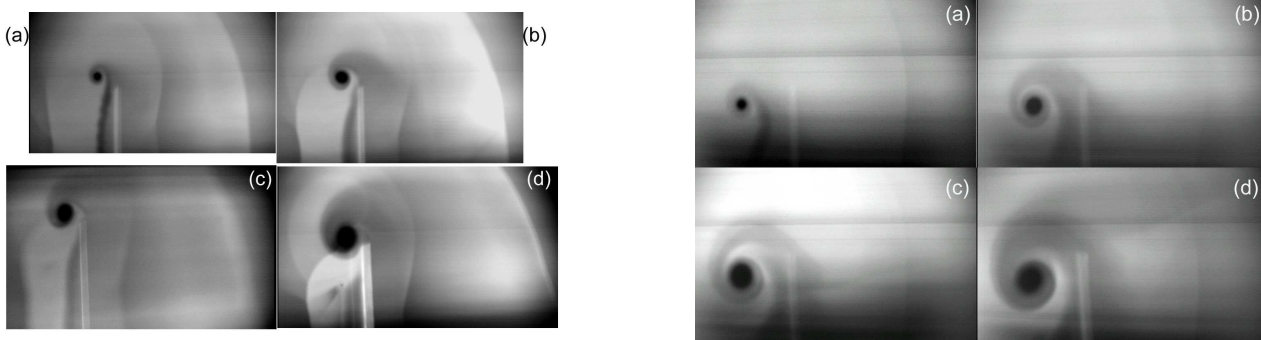


Figure 7: Laser sheet visualization at $M = 3$, $x/b = 1.5$ (left) and 3 (right): (a) $\alpha = 5$ deg, (b) $\alpha = 10$ deg, (c) $\alpha = 15$ deg, (d) $\alpha = 20$ deg.

Figure 7 shows typical images obtained with the laser sheet technique. In these figures, the vortex core is seen as a black region. In the near wake ($x/b = 1.5$) the laser sheet images has revealed a complicated flowfield structure with formations of the bow shock, inner shocks and expansion waves. The observed flowfield is similar to the flow topology over a rectangular wing which was described by Borovoy.¹⁷ In the far wake ($x/b = 3$) only the bow shock and the vortex sheet which roll-up of the vortex core are visible. Inner shocks and expansion waves are dissipated. Results of visualization allowed us to determine the size and position of the vortex core at different distances from the trailing edge of the wing.

Figure 8 shows typical results of 5-hole pressure probe measurements. These measurements yielded detailed data on the fields of total pressure, Mach number, and Mach number components onto the axes of the flow-fitted coordinate system. A comparison of visualization and probing results showed that the vortex core, which looks as a dark region in the laser sheet images, is characterized by a decrease in total pressure, Mach number, and axial component of velocity; thus, a wake-type profile is formed. The maximum values of the circumferential velocity correspond to the edge of the vortex-core (Fig. 8 c).

Figure 9 shows Euler solutions for the case of $M = 3$ and $\alpha = 10$ deg. Nondimensional contours of density and Pitot pressure as well as Mach number contours are presented. Bow shock wave, inner shock and vortex core are clearly visible. Thus, Euler solution as a whole predicts qualitative flow pattern in the wing wake reasonably well. But in Fig. 9b the vortex core corresponds to the region with large Mach number. It contradicts the experimental results, where the minimum in Mach number was observed. Nondimensional Pitot pressure distributions through the vortex core are given in Fig. 10a. Numerical data to each set of equations and experimental data are presented. For this

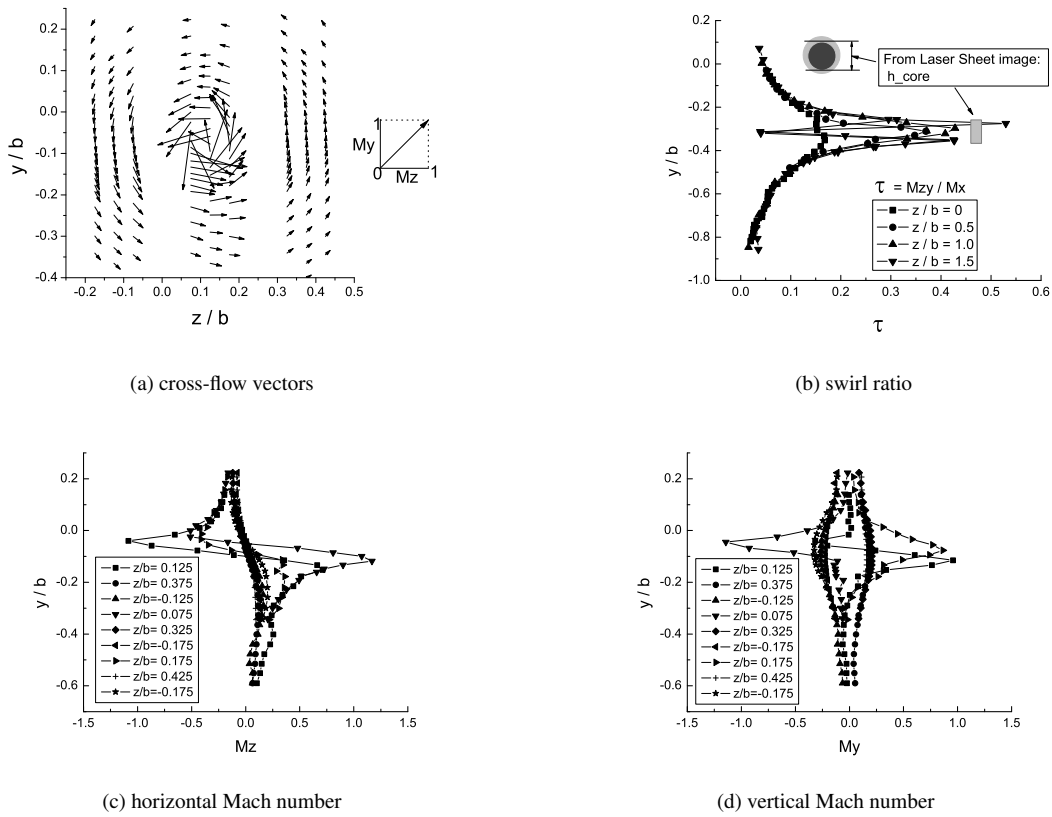


Figure 8: Five-hole pressure probe data.

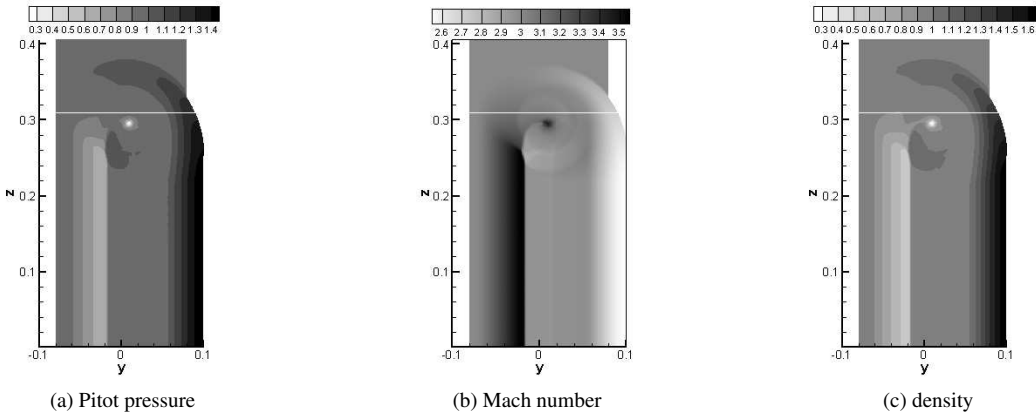


Figure 9: Euler solution for $M = 3$ and $\alpha = 10$ deg at $x/b = 1.5$

and the remaining figures, the origin of the vertical axis has been shifted to the vortex center of each distribution so that profiles can be compared spatially with respect to center of the vortex core. The vortex core center is defined on minimum of both Pitot pressure and crossflow Mach number (Fig. 10). As is obvious Euler and laminar Navier-Stokes solutions produced similar Pitot pressure distributions with noticeable loss in the vortex core. Computational data are close to those obtained in the experiments outside the vortex core ($|Y - Y_C| \geq 0.05$). But inside the vortex core the computational Pitot pressure is twice higher than the corresponding experimental data.

Figure 10c shows Mach number distributions through the vortex core. A clearly defined wake-like profile with a minimum of the Mach number is obtained in experiments and Navier-Stokes solution. In contrast to that Euler solution revealed a jet-like profile with a maximum of the Mach number at the vortex axis. Figure 10b shows crossflow Mach number distributions through the vortex core. As stated above the crossflow Mach number is a good estimate of circumferential Mach number. In experiments and both sets of computations classical profiles with their maxima at

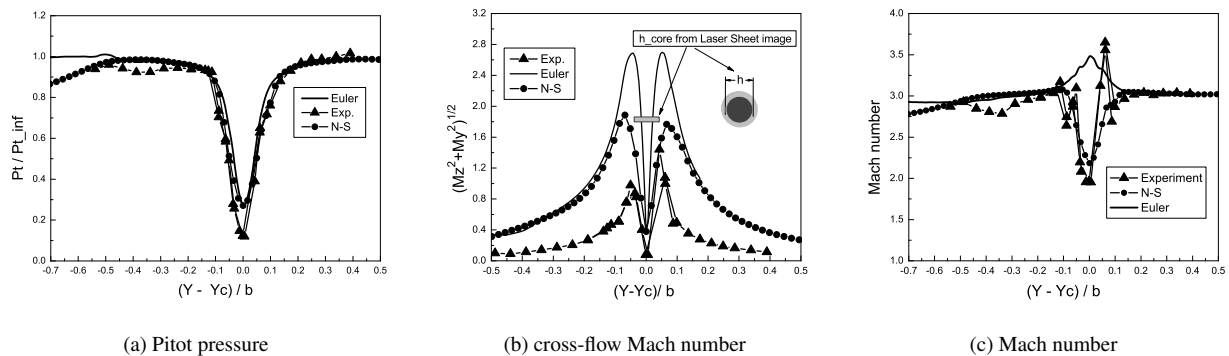


Figure 10: Numerical and experimental flow field data through the vortex core

the vortex core edge are obtained. The tangential velocity varies nearly linearly from approximately zero to maximum in the vortex core. In the outer region of the vortex core tangential velocity varies with r^{-1} (where r – distance from the vortex core axis), and asymptotically approaches zero. As mentioned above the vortex core edge is defined on maximum of the crossflow (circumferential) Mach number. Figure 10b indicates that the Euler solution can predict the vortex core size sufficiently well while the Navier-Stokes solution produces a vortex core size somewhat larger than one obtained in the experiments and Euler computations. Figure 10b also shows significant differences in maximum values of crossflow Mach number obtained in the experiments and both sets of computations. The Euler solution gets this value two times higher than one obtained in the experiments. The Navier-Stokes solution produced more reliable data, which nevertheless considerably exceed experimental ones.

Acknowledgements

The work was supported by the Russian Foundation for Basic Research (grant No. 06-01-00774) and performed under the contract with the International Science and Technology Center (ISTC), Moscow.

References

- [1] A. Stanbrook, L.C. Squire. Possible types of flow at swept leading edges. *Aeronaut. Quart.*, **15**, 72–82, 1964.
- [2] Wood R.M., Miller D.C. Leaside flow over delta wings at supersonic speeds. *J. of Aircraft*, **21**, 680–686, 1984.
- [3] Y.K. Narayan, S.N. Seshadri. Types of flow on the lee side of delta wings *Prog. in Aerospace Sci.*, **33**, 167–257, 1997.
- [4] M.D. Brodetsky, A.M. Kharitonov, E. Krause, S.B. Nikiforov, A.A. Pavlov, A.M. Shevchenko. Supersonic Lee-side Flow Topology Revisited. *Experiments in Fluids*, **29**, 592–604, 2000.
- [5] M.D. Brodetsky, E. Krause, S.B. Nikiforov, A.A. Pavlov, A.M. Kharitonov, A.M. Shevchenko. Evolution of vortex structures on the leeward side of a delta wing. *J. of Applied Mech. and Techn. Phys.*, **42**, 243–254, 2001.
- [6] Smart M, Kalkhoran I and Bentson J. Measurements of supersonic wing tip vortices. *AIAA Journal*, Vol. 33, No. 10, pp 1761–1768, 1995.
- [7] Brodetsky M. and Shevchenko A. An experimental study of supersonic flow on the leeward side of a delta wing. *Thermophysics and Aeromechanics* Vol. 5, No. 3, pp 281–291, 1995.
- [8] M.D. Brodetsky, A.V. Zabrodin, A.E. Lutsky, A.M. Kharitonov, A.M. Shevchenko. Numerical and experimental investigations of a supersonic flowfield on the leeward side of a delta wing. *Aeromechanics and Gasdynamics*, Vol. 1, pp. 3–12, 2002 (in Russian).
- [9] Shevchenko A.M., Kavun I.N., Pavlov A.A., Zapryagaev V.I. Review of ITAM experiments on shock / vortex interaction. In *European Conference for Aerospace Sciences, Moscow, July 4-7, 2005*, Paper No. 2.07.01., 2005

- [10] Shevchenko A.M., Kavun I.N., Pavlov A.A., Zapryagaev V.I. Visualization of wing-tip vortices and of an unsteady flowfield in shock / vortex interaction. In *12th Intern. Symp. on Flow Visualization Gottingen, Germany, September 10-14, 2006*, ISBN 0-9533991-8-4, Paper No. 219, pp. 1-10, 2006.
- [11] G.P. Voskresensky, A.E. Lutsky, M.G. Orlova. Supersonic flow past the side part of the wings with a wedge-shaped profile with a shock wave attached to the leading edge. *Preprint No. 62, Keldysh Inst. Appl. Math., Russian Acad. Sci., Moscow, 1985* (in Russian).
- [12] O.A. Kandil, A.H. Chuang. Influence of numerical dissipation on computational Euler equations for vortex-dominated flows. *AIAA J.*, **25**, 1426–1434, 1987.
- [13] E.M. Murman, K.G. Powell, A.M. Goodsell, M. Landahl. Leading-edge vortex solution with large total pressure losses. *AIAA Paper*, **39**, 1987.
- [14] K.G. Powell, Murman E.M., Perez E.S., Baron J.R. Total pressure loss in vortical solutions of the conical Euler equations. *AIAA J.*, **25**, 360–368, 1987.
- [15] McMillin S.N., Thomas J.L., Murman E.M. Euler and Navier-Stokes solution for the lee side flow over delta wings at supersonic speeds. *AIAA Paper*, **2270**, 1987.
- [16] R.W. Newsome. Euler and Navier-Stokes solution for flow over conical delta wings. *AIAA Journal*, **24**, 552–561, 1986.
- [17] Borovoy V. Flowfield and heat transfer in the regions of shock wave / boundary layer interaction. *Moscow: Mashinostroenie*, 1983, (in Russian).
- [18] Borovoy V, Kubishina T, Skuratov A and Yakovleva L. Vortex in a supersonic flow and its influence on a flowfield and heat transfer of the blunted body. *Mechanica zhidkosti i gaza*, No. 5, pp 66–76, 2000, (in Russian).



This page has been purposely left blank